Top Curr Chem (Z) (2016) 374:33
DOI 10.1007/s41061-016-0031-5

REVIEW

Organic Light-Emitting Devices with Tandem Structure

Takayuki Chiba[1] · Yong-Jin Pu[1] · Junji Kido[1]

Received: 14 January 2016 / Accepted: 25 April 2016 / Published online: 12 May 2016

Abstract Tandem organic light-emitting devices (OLEDs) have attracted considerable attention for solid-state lighting and flat panel displays because their tandem architecture enables high efficiency and long operational lifetime simultaneously. In the tandem OLED structure, plural light-emitting units (LEUs) are stacked in series through a charge generation layer (CGL) and an electron injection layer (EIL). In this chapter, we focus on the key features of tandem OLEDs for high efficiency and long operational lifetimes. We also demonstrate the effect of the CGL comprising a Lewis acid, an n-type semiconductor metal oxide, and an organic electron-accepting material. We discuss the two types of EILs in tandem OLEDs: alkali metals containing *n*-type compounds and ultra-thin metals. Finally, we focus on the recent progress of the state-of-the-art solution-processed tandem OLEDs.

Keywords Tandem · Charge generation layer · p-n junction

1 Introduction

Organic light-emitting devices (OLEDs) have attracted considerable interest for use in flat panel lighting and thin film displays [1–7]. The operational lifetime of OLEDs decreases with increasing current density or luminance because the large

This article is part of the Topical Collection "Photoluminescent Materials and Electroluminescent Devices"; edited by Nicola Armaroli, Henk Bolink.

✉ Yong-Jin Pu
pu@yz.yamagata-u.ac.jp

✉ Junji Kido
kid@yz.yamagata-u.ac.jp

[1] Department of Organic Device Engineering, Research Center for Organic Electronics, Yamagata University, 4-3-16 Jonan, Yonezawa, Yamagata 992-8510, Japan

number of holes and electrons passing through the organic layer causes electrochemical side-reactions of organic compounds [8]. A particular approach to solve this issue is the use of tandem OLEDs, which have been fabricated to attain long operational lifetimes under high luminance [9–15]. In a tandem OLED structure, plural light-emitting units (LEUs) are stacked in series through interconnecting layers such as a transparent conductive layer (TCL) [9] or a charge generation layer (CGL) [11]. In addition, electron injection layers (EILs) are also important to reduce the electron injection barrier from the TCL or CGL into the first LEU [16–20]. Under an identical current density, compared with a single LEU device, tandem OLEDs with two LEUs can exhibit a two-fold increase in luminance. Therefore, the efficiency and operational lifetime of tandem OLEDs can also be improved in comparison with those of conventional single unit OLEDs. In Sect. 2, we will review the key features of tandem OLEDs for high efficiency and long operational lifetimes. In Sect. 3, we will demonstrate the effect of interconnecting layers such as TCLs and CGLs. In Sect. 4, we will focus on two types of EILs: alkali metals containing *n*-type compounds and ultra-thin metals. Finally, in Sect. 5, we will demonstrate recent progress in the tandem OLEDs with solution processing fabrication of LEUs, EILs, TCLs, and CGLs.

2 Tandem OLEDs

In conventional OLEDs, the luminance increases with the current density. However, the operational lifetime decreases with increasing current density because the charge passing through the organic layer causes degradation of the organic material. Thus, it is quite difficult to simultaneously obtain high luminance and long operational lifetimes when using a high current density. To overcome this critical issue, Kido et al. reported tandem OLEDs comprising multiple LEUs vertically stacked with an EIL and an interconnecting layer in 2003 [9]. Since then, various types of tandem OLEDs have been reported [10–15]. The conventional structure of a tandem OLEDs is shown in Fig. 1. In a tandem structure, multiple emissions can be obtained from each stacked LEU. As compared to conventional OLEDs with a single LEU at an identical current density, when two LEUs are serially stacked in tandem OLEDs, the luminance and driving voltage increases two-fold. Therefore, the current efficiency (cd/A) and external quantum efficiency of the tandem OLEDs can be increased two-fold when compared with the efficiency of a single LEU device. However, identical power efficiency (lm/W) is observed for both tandem OLEDs and singe LEU devices. As a result, due to decreased current density in each LEU, at the same luminance, the operational lifetime of tandem OLEDs can be longer than that of a single LEU [12, 15]. In other words, tandem OLEDs can avoid the critical trade-off between luminance and operational lifetime. Adjustment of optical interference in the device is also very important in order to achieve tandem efficiencies [13, 14]. In particular, due to phase matching, optical distances from the emissive zone in individual LEUs to reflecting metal electrodes such as Al must be set within a

specific range of $\lambda/4n$ multiplied by an odd number, where λ is the emission wavelength and n is the refractive index.

Tandem OLEDs offer the following advantages: (1) Easy control of the color temperature and color-rendering index for white light-emitting devices because blue, green and red emission can be separately obtained from each LEU; (2) The greater thickness (>300 nm) of tandem OLEDs results in fewer short-circuit defects; (3) A low current density can avoid roll-off of the efficiency, which is especially important for devices with phosphorescent emitters.

3 Interconnecting Layers in Tandem OLEDs

3.1 Transparent Conductive Layer

The use of a transparent, conductive indium tin oxide (ITO) electrode as an interconnecting layer is one approach to stacking LEUs in series. An interconnecting ITO layer can be deposited using a facing-target type sputtering method [9]. Ultra-thin metals such as aluminum (Al), silver (Ag) and gold (Au) have also been utilized as interconnecting layers [21–24]. Electrons are injected from a conductive ITO or an ultra-thin metal electrode into the lowest unoccupied molecular orbital (LUMO) level of the compounds in the 1st LEU. Holes are supplied from ITO or an ultra-thin metal into the highest occupied molecular orbital (HOMO) level of the

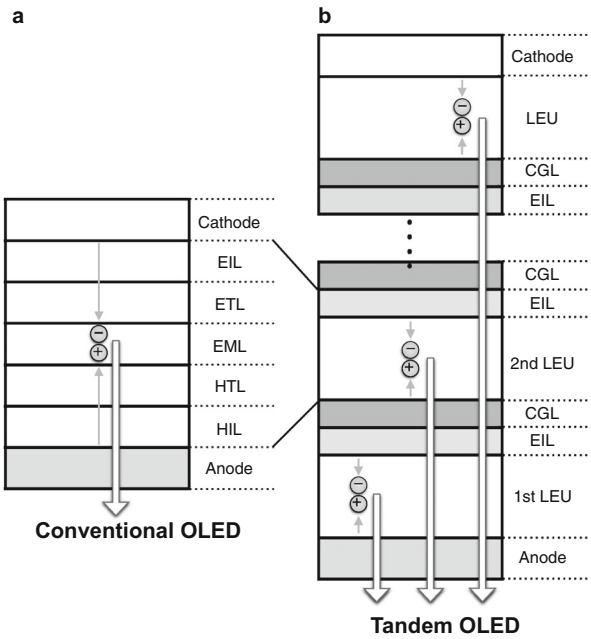

Fig. 1 Device structure of **a** a conventional OLED and **b** a tandem OLED

compounds in the 2nd LEU. Tandem OLEDs composing two fluorescent-based LEUs and an interconnecting ITO layer have been demonstrated, and they exhibit a current efficiency of 34 cd/A and an external quantum efficiency of 10 %. A doubled efficiency was observed when compared with a conventional single LEU device (current efficiency of 17 cd/A and external quantum efficiency of 5 %). However, the ITO layer deposited using a sputtering method often results in serious damage to the organic layer. If the conductivity of ITO or an ultra-thin metal is too high, crosstalk can occur between each emitting pixel in display applications. In addition, a metal-based interconnecting layer may decrease transmittance in the visible region [22, 23].

3.2 Charge Generation Layer Comprising an Electron-Accepting and an Electron-Donating Material

Instead of ITO and ultra-thin metals, a charge generation layer (CGL) comprising an electron-accepting and an electron-donating layer can be employed as an interconnecting layer. The lateral conductivity of the CGL is sufficiently low and is almost insulating. In general, the electron-accepting components of CGLs can be categorized into three types: (1) Lewis acids such as iron chloride ($FeCl_3$) [10] and tetrafluorotetracyanoquinodimethane (F_4TCNQ) [9, 12, 20, 25–27]; (2) *n*-type semiconductor metal oxides such as vanadium oxide (V_2O_5) [9, 28, 29], molybdenum oxide (MoO_3) [11, 12, 30–36], tungsten oxide (WO_3) [12, 18, 37], and rhenium oxide (ReO_3) [38]; and (3) electron-accepting organic compounds such as hexaazatriphenylene hexacarbonitrile ($HATCN_6$) [12–15, 25, 39–44]. Conversely, hole-transporting arylamine compounds such as *N*,*N*′-di(naphthalene-1-yl)-*N*,*N*′-diphenylbenzidine (NPD), *N*,*N*′-bis(3-methylphenyl)-*N*,*N*′-diphenylbenzidine (TPD), and 4,4′-cyclohexylidenebis(*N*,*N*-bis(4-methylphenyl)benzenamine) (TAPC), 4,4′,4″-tris(*N*-carbazolyl)-triphenyl amine (TCTA) can be used as an electron-donating layer as shown in Fig. 2. The mechanism of charge generation in the bilayers of the

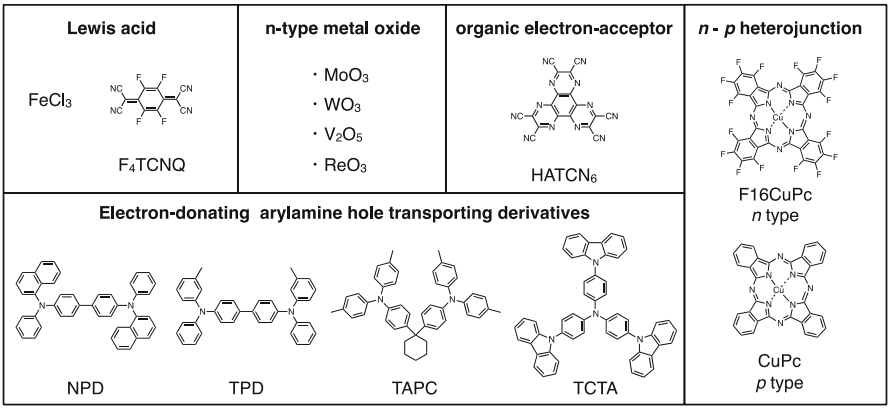

Fig. 2 Chemical structure of electron-accepting and electron-donating materials used in CGLs

electron-accepting and electron-donating layers has previously been investigated in detail. Interface energetic dynamics can be determined using ultraviolet photoelectron spectroscopy (UPS) and inverse photoemission spectroscopy (IPES). MoO_3 shows a deep conduction band of 6.7 eV and a high work function of 6.9 eV [45]. This result indicates that MoO_3 acts as an *n*-type semiconductor material. Another metal oxide WO_3 can also play a role as an *n*-type semiconductor because of its high work function (6.7 eV). UPS and IPES measurements of CGL comprising WO_3 and hole-transporting TCTA exhibit a large interfacial dipole of 1.5 eV and quite a small energy difference of 0.8 eV between the conduction band of WO_3 and the HOMO level of TCTA [46]. Thus, charge generation (or electron-pulling) occurs at the interface between the electron-accepting layer (WO_3) and electron-donating layer (TCTA).

Lewis acids such as $FeCl_3$ and F_4TCNQ have a strong electron-accepting property and form a charge-transfer (CT) complex with electron-donating arylamine compounds such as NPD or TPD [9]. Absorption in the near-infrared region from 800 to 2000 nm has been observed, indicating the formation of a CT complex and charge generation. However, these Lewis acids are not stable and cause increased driving voltage during long-term operation. In addition, it is difficult to handle them using vacuum evaporation in device fabrication due to contamination, corrosivity, and optical absorption.

Conversely, *n*-type semiconductors such as V_2O_5, MoO_3, WO_3, and ReO_3 are more convenient for use as an electron acceptor due to a high transmittance of 85–90 % in the visible region, less corrosivity, and greater electrochemical stability than Lewis acids [11]. The conduction band of a metal oxide is less than 7 eV, easily accepting electrons from the HOMO level of hole-transporting arylamines: TPD (5.4 eV) [28], NPD (5.5 eV) [11], and TAPC (5.6 eV) [35]. These metal oxides can act as an electron acceptor in a metal oxide-doped organic layer. However, regarding the evaporation temperatures of metal oxides, with the exception of ReO_3 (340 °C), the rest are relatively high (over 600 °C), resulting in complicated problems in a mass production line [38].

An organic acceptor compound, $HATCN_6$, has been employed as a substitute for a Lewis acid or a metal oxide in the CGL of tandem OLEDs. $HATCN_6$ can be evaporated in vacuum at a relatively low temperature below 300 °C, sufficiently lower than those of metal oxides. This is an advantage for device fabrication. $HATCN_6$ has no absorption in the visible region due to a large energy gap [39]. The LUMO level of $HATCN_6$ is close to the HOMO level of electron-donating arylamine compounds [47]. Thus, $HATCN_6$ can accept one electron from the HOMO level of an adjacent donor compound such as NPD or TAPC [12, 13]. Although $HATCN_6$ is an organic compound, it exhibits electrochemical stability as high as that of metal oxides. Tandem OLEDs with $HATCN_6$ used as the CGL have been reported to show excellent operational lifetimes and can suppress increasing driving voltages [12, 28, 39, 42]. The device performance of tandem OLEDs with various CGLs are summarized in Table 1.

The *n*- and *p*-type organic heterojunction of a copper hexadecafluorophthalocyanine (F_{16}CuPc) and a copper phthalocyanine (CuPc) bilayer have been reported as another strategy for the CGL [48]. F_{16}CuPc and CuPc have been used as electron-accepting (*n*-type) and electron-donating (*p*-type) compounds. The charge generation mechanism can be explained as follows: an interfacial dipole is formed at the interface between F_{16}CuPc and CuPc, which causes energy level alignment; therefore, an electron is injected from CuPc into F_{16}CuPc. Similarly, F_{16}CuPc and CuPc can be replaced with fullerene (C_{60}) and pentacene, respectively, which has also been reported as a CGL in tandem OLEDs [49–51].

Table 1 Device performances of the tandem OLEDs using several types of CGLs

CGL	Process	Material type	Emitter	References
ITO	Evaporation	Metal oxide electrode	Green fluorescent	[9]
V_2O_5/NPD	Evaporation	Metal oxide	Green fluorescent	[9]
			White fluorescent	[29]
MoO_3/NPD	Evaporation	Metal oxide	Green fluorescent	[12, 30]
			White fluorescent	[32, 33]
			White phosphorescent	[11, 31]
MoO_3/TCTA	Evaporation	Metal oxide	Green phosphorescent	[34]
WO_3/NPD	Evaporation	Metal oxide	Green fluorescent	[12]
			White fluorescent	[37]
WO_3/TCTA	Evaporation	Metal oxide	Green phosphorescent	[18]
ReO_3/NPD:ReO_3	Evaporation	Metal oxide	Green phosphorescent	[38]
NPD:F_4-TCNQ	Evaporation	Lewis acid	Green fluorescent	[9, 12]
			Green phosphorescent	[25]
NPD:$FeCl_3$	Evaporation	Lewis acid	Green phosphorescent	[10]
mMTDATA:F_4-TCNQ	Evaporation	Lewis acid	Green fluorescent	[16]
TPD:F_4-TCNQ	Evaporation	Lewis acid	Green fluorescent	[26]
$HATCN_6$/NPD	Evaporation	Organic acceptor	Green fluorescent	[12]
			Green phosphorescent	[13, 25]
			Blue phosphorescent	[15]
$HATCN_6$/TAPC	Evaporation	Organic acceptor	White phosphorescent	[14]
Ag or Au	Evaporation	Metal electrode	Green fluorescent	[21]
Al/WO_3/Au	Evaporation	Metal electrode	Green fluorescent	[22, 23]
F_{16}CuPc/CuPc	Evaporation	p-n heterojunction	Blue fluorescent	[48]
C60/Pentacene	Evaporation	p-n heterojunction	Green fluorescent	[49]
C60/CuPc	Evaporation	p-n heterojunction	Red phosphorescent	[50]
MoO_3/Poly-TPD	Hybrid	Metal oxide	Yellow fluorescent	[77]
WO_3/PEDOT:PSS	Solution	Metal oxide	Yellow fluorescent	[86]
PMA/TFB	Solution	Heteropoly acid	Yellow fluorescent	[89]
PEDOT:PSS	Solution	Conductive polymer	White phosphorescent	[92]

4 Electron Injection Layer (EIL) in Tandem OLEDs

4.1 Alkali Metal Containing *n*-Type Dopant

In general, conventional electron-accepting compounds such as metal oxides or $HATCN_6$ have a fairly deep conduction band of 6.5–6.7 eV [45, 46] or LUMO level of 6.0 eV [47], respectively. A generated electron in the CGL is difficult to be injected into the LUMO level of the compound in the first LEU. Thus, electron injection from the CGL into the first LEU is a critical factor for reducing the driving voltage and improving the efficiency of tandem OLEDs. For effective electron injection from the CGL into the first LEU, the approach where a low work–function alkali metal, such as lithium (Li) [10–12], cesium (Cs) [9], calcium (Ca) [52], magnesium (Mg) [17], is doped into an electron-transporting material, such as 4,7-diphenyl-1,10-phenanthroline (BCP), 4,7-diphenyl-1,10-phenanthroline (Bphen), or tris(8-hydroxyquinolinato)aluminium (Alq_3), has been widely used as an *n*-doped EIL (Fig. 3). Moreover, the energy level at the interface between the EIL and CGL can be determined using UPS and IPES. During the gradual evaporation of an alkali metal-doped electron-transporting layer onto the CGL, the work–function dramatically decreases because of the formation of the space charge effect, which results in the energy level alignment at interfaces between the EIL and CGL as shown in Fig. 4. These alkali metals exhibit high reactivity to atmospheric oxygen and moisture and are easily diffused into the organic layer, which results in device degradation. Alkali metal carbonates such as cesium carbonate (Cs_2CO_3) [18, 30] or rubidium carbonate (Rb_2CO_3) [14, 38] are less sensitive to air and can, thus, be commonly used as more stable *n*-type dopants. However, alkali metals and their carbonates require a high evaporation temperature compared with conventional organic compounds. Another type of cesium compound, cesium azide (CsN_3) [19, 34] has been introduced as an efficient *n*-type dopant in the EIL of tandem OLEDs, with air stability and a low evaporation temperature of 310 °C. In similar concepts for a stable *n*-type dopant with a low deposition temperature, lithium amide ($LiNH_2$)

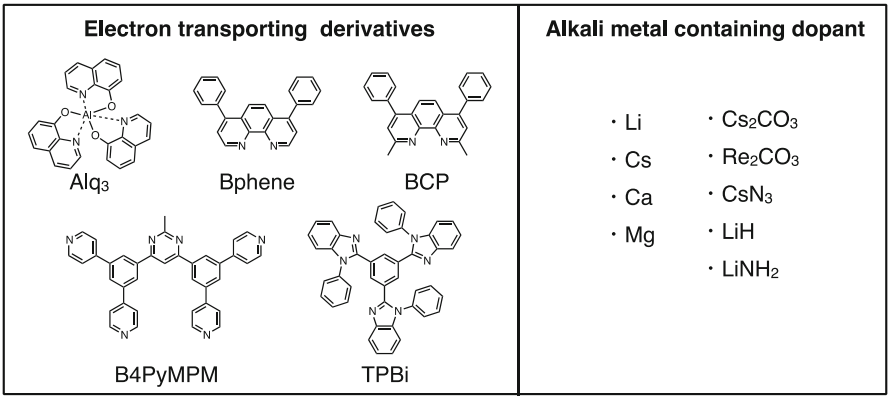

Fig. 3 Chemical structure of electron-transport compounds and alkali metal-containing dopants

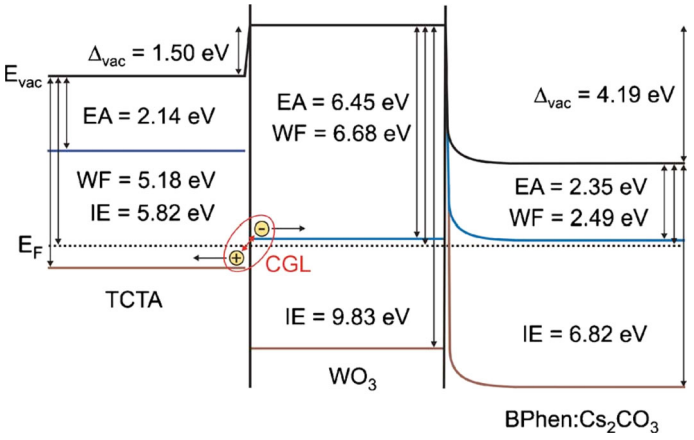

Fig. 4 Energy level alignment in the CGL and EIL. Reproduced with permission from [46]. Copyright 2010, AIP Publishing LLC

[42] and lithium hydride (LiH) [44] are also effective in tandem OLEDs, along with other alkali metals, alkali metal carbonates, and azide compounds. The device performance of various EIL in tandem OLEDs are summarized in Table 2.

4.2 Ultra-Thin Bilayer of Metal and Alkali Metal Halide

In conventional OLEDs, alkali metal halides such as lithium fluoride (LiF) have been commonly used in the EIL to dramatically reduce the electron injection barrier from the Al cathode into organic layers [53, 54]. An ultra-thin (less than 2 nm) bilayer of LiF and Al can be utilized as an effective EIL adjacent to the CGL in tandem OLEDs [13, 24, 55]. In rubrene-based yellow fluorescent tandem OLEDs with the EIL comprising an ultra-thin bilayer of LiF and Al, when compared with a single LEU device, a doubled current efficiency and a long operational lifetime was exhibited [13]. This ultra-thin bilayer can be used in the application of various types of electron-transporting materials. When a high triplet energy level and a wide gap electron-transporting material bis-4,6-(3,5-di-4-pyridylphenyl)-2-methylpyrimidine (B4PYMPM) was used as the ETL in green phosphorescent tandem OLEDs, an extremely high current efficiency of 250 cd/A was achieved as shown in Fig. 5. Lithium phenolate complexes such as 8-quinolinolato lithium (Liq) are also well-known electron injection materials [56, 57]. These complexes can be evaporated using a relatively low temperature and are much less sensitive to the thickness when compared with insulating LiF. Electron injection from the CGL into the LEU assisted by an ultra-thin bilayer has been studied in detail [20]. The evaporated Al reacts with LiF or Liq, leading to *n*-type doping at the surface of the ETLs. A high external quantum efficiency of over 40 % was obtained using an ultra-thin bilayer of Liq and Al as the EIL in blue phosphorescent tandem OLEDs [35]. Due to the case of handling and its high stability, this ultra-thin bilayer is a good candidate for replacing highly reactive alkali metals or alkali metal carbonates as *n*-type dopants.

Table 2 Device performances of the tandem OLEDs using several types of EILs

EIL	Process	Material type	Emitter	References
BCP:Cs	Evaporation	Metal oxide	Green fluorescent	[9]
Alq_3:Mg	Evaporation	Alkali metal	Green fluorescent	[16, 26]
			White fluorescent	[37]
Alq_3:Li	Evaporation	Alkali metal	Green phosphorescent	[10]
			Green fluorescent	[12]
			Blue phosphorescent	[15]
BCP:Li	Evaporation	Alkali metal	White fluorescent	[29]
Bphen:Mg	Evaporation	Alkali metal	Green fluorescent	[17]
Bphen:Li	Evaporation	Alkali metal	White phosphorescent	[11, 31]
			Green phosphorescent	[25]
Alq_3:Ca	Evaporation	Alkali metal	Green fluorescent	[52]
Alq_3:Cs_2CO_3	Evaporation	Metal carbonate	Green fluorescent	[30]
Bphen:Cs_2CO_3	Evaporation	Metal carbonate	White fluorescent	[32]
			Green phosphorescent	[18]
BCP:Cs_2CO_3	Evaporation	Metal carbonate	White fluorescent	[33]
Bphen:Rb_2CO_3	Evaporation	Metal carbonate	Green phosphorescent	[38]
B3PyMPM:Rb_2CO_3	Evaporation	Metal carbonate	White phosphorescent	[14]
LiF/Al	Evaporation	Alkali halide, metal	Green fluorescent	[21, 23]
			Green phosphorescent	[13]
Liq/Al	Evaporation	Alkali halide, metal	Green phosphorescent	[20]
			Blue phosphorescent	[35]
Bphen:CsN_3	Evaporation	Metal azide	Green fluorescent	[19]
			Green phosphorescent	[34]
Alq_3:LiH	Evaporation	Alkali metal hydride	Green fluorescent	[42]
Bphen:$LiNH_2$	Evaporation	Alkali metal amide	Green fluorescent	[44]
ZnO/Al	Hybrid	Metal oxide, metal	Yellow fluorescent	[77]
ZnO/PEI	Solution	Modified metal oxide	Yellow fluorescent	[86]
ZnO/PEIE	Solution	Modified metal oxide	Yellow fluorescent	[89]
			White phosphorescent	[92]

5 Solution-Processed Tandem OLEDs

5.1 Solution- and Evaporation-Processed Hybrid Tandem OLEDs

The vacuum evaporation method is predominantly used in the fabrication process of tandem OLEDs because multilayer structures with more than eight layers between the anode and cathode are required. The vacuum evaporation process can easily form multilayer structures for devices. However, solution-processing techniques for OLED fabrication, such as spin-coating, die-coating, and inkjet printing, have attracted great attention due to the low fabrication cost and potential for large coated

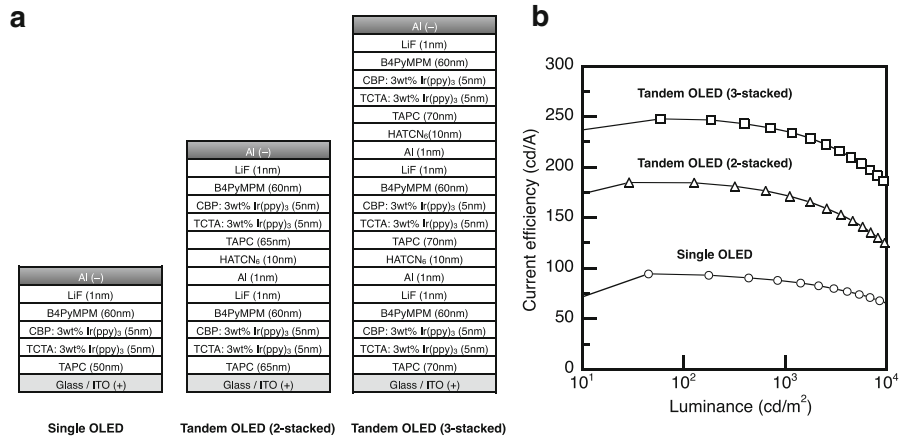

Fig. 5 **a** Device structures of a single-OLED, a two-stacked tandem OLED and a three-stacked tandem OLED. **b** The current efficiency–luminance characteristics of the devices. Reproduced with permission from [13]. Copyright 2011, Elsevier

areas [58–60]. It is not easy to fabricate a multilayer structure using a solution-processing technique because coating solvents can dissolve the bottom organic layer [61–66]. Although the use of an orthogonal solvent technique is an important factor in achieving multilayer structures, metals or alkali metal halides are difficult to apply in solution-processing techniques due to their poor solubility in common organic solvents. However, solution-processed electron injection materials are absolutely imperative in the development of solution-processed tandem OLEDs. The alkali metal carbonate Cs_2CO_3 has been widely used as a solution-processed electron injection compound [67–69]. Recently, an *n*-type metal oxide of zinc oxide (ZnO) nanoparticles has been applied to solution-processing at a low temperature [70–72]. A mixture of ZnO and Cs_2CO_3 has been also employed to improve the electron injection property [72–76].

There are a few reports on the solution and evaporation hybrid fabrication processing technique for tandem OLEDs with a two-fold stacked LEU comprised of hole injection, light-emitting, and electron injection layers [77–79]. The addition of poly(4-vinyl pyridine)—PVPy—as a polymer binder into the ZnO:Cs_2CO_3 layer improved the film morphology without compromising the device properties, and ZnO:Cs_2CO_3:PVPy was used as a solution-processed EIL in hybrid tandem OLEDs. Electron-accepting MoO_3 and ultra-thin Al were deposited using vacuum evaporation. The evaporated MoO_3 layer is insoluble in common organic solvents such as toluene and dichlorobenzene. Subsequently, a hole-transporting arylamine polymer [poly(4-butylphenyl-diphenyl-amine); poly-TPD], was spin-coated onto MoO_3 from a dichlorobenzene solution. The current efficiency of the hybrid tandem OLEDs was 10 cd/A, which was the sum of the efficiency of each LEU (Fig. 6). These results indicate that the bilayer of MoO_3 and poly-TPD operated effectively as a CGL.

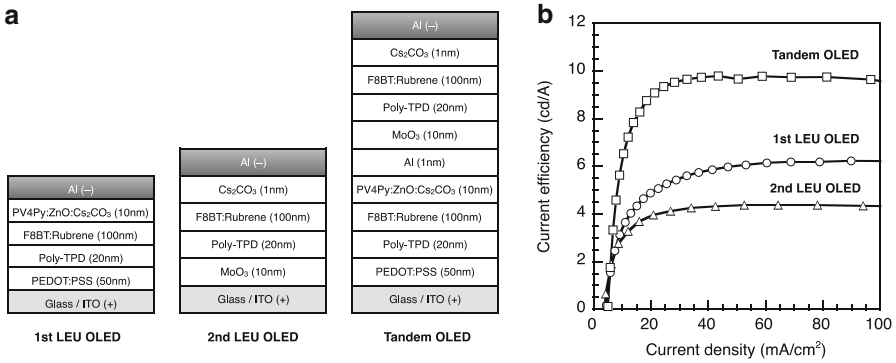

Fig. 6 **a** Device structure of the 1st LEU OLED, 2nd LEU OLED, and solution-evaporation hybrid tandem OLED. **b** Current efficiency–current density characteristics of the devices. Reproduced with permission from [77]. Copyright 2012, The Royal Society of Chemistry

5.2 Solution-Processed Tandem OLEDs with a Fluorescent Polymer

The fabrication of completely solution-processed tandem OLEDs is largely dependent on the availability of alternative solution-processable materials to replace MoO_3 and ultra-thin metals. In particular, the interconnecting layer comprising CGL and EIL materials has to not only be formed from solution without dissolving the bottom layer but also be insoluble to coating solvents for subsequent upper layers. In addition, a low annealing temperature is required for the processing of the interconnecting layer to suppress thermal influence on the bottom LEUs. Aliphatic amine-based polymers such as polyethyleneimine (PEI) and polyethyleneimine-ethoxylated (PEIE), or a bilayer of ZnO and PEI (or PEIE) have been used as solution-processable EILs in OLEDs because these amine polymers reduce the work function of ZnO and electrodes such as ITO due to the interfacial dipole effect [80–83]. In contrast, various metal oxides such as WO_3 and NiO_x have been studied as solution-processed HILs [84, 85].

Recently, solution-processed fluorescent polymer tandem OLEDs were successfully fabricated with an inverted or regular structure comprising ZnO modified with PEI and WO_3 [86, 87]. Moreover, the solution-processed tandem OLEDs with a regular structure using PEIE and ZnO nanoparticles as an EIL and phosphomolybdicacid hydrate $(MoO_3)_{12}{\cdot}H_3PO_4{\cdot}(H_2O)_x$ (PMA) [88] as the electron-accepting material of the CGL have been fabricated [89]. A bilayer of ZnO and PEIE was coated onto the fluorescent light-emitting polymer [poly(9,9-dioctylfluorene-*alt*-benzothiadiazole); F8BT] from 2-ethoxyethanol dispersion and solution, respectively. It is required that these EILs not be soluble in the solvent used for coating subsequent upper layers, i.e., the *p*-type electron-accepting layer and hole-transporting layer in the CGL. Therefore, the coating solvent of the PMA, which is a *p*-type electron-accepting layer, cannot be a polar solvent such as water or alcohol because they easily dissolve the PEIE underlayer. PMA is soluble in acetonitrile, whereas PEIE, ZnO, and F8BT are not soluble in acetonitrile.

Furthermore, poly(9,9-dioctyl-fluorene-*co*-*N*-(4-butylphenyl)-diphenylamine)—TFB—was chosen as the HTL of the 2nd LEU. In the coating of TFB, *p*-xylene is chosen because it does not dissolve PMA, PEIE, or ZnO. An appropriate choice of solvents during the coating of each layer ensures that the nine-layer stacked structure can be produced using solution-based processes (Fig. 7a). The driving voltage and current efficiency of the solution-processed tandem OLEDs were the sums of the values of each individual LEU (Fig. 7b, c). These results indicate that a CGL comprising PMA and TFB fabricated using a solution-based process successfully generates electrons and holes under an applied voltage. These generated electrons are efficiently injected into the 1st LEU through the ZnO/PEIE bilayer and the holes are injected into the 2nd LEU. In addition, even with two-fold higher luminance, the operational lifetime of tandem OLEDs exhibited a similar degradation tendency to that of an individual single LEU device (Fig. 7d).

5.3 Solution-Processed Phosphorescent Tandem OLEDs

Section 5.2 described solution-processed tandem OLEDs. The LEUs were limited to fluorescent π-conjugated polymers such as "Super Yellow" [86] or F8BT [89] because their much lower solubility in organic solvents compared with that of small-molecule materials was an advantage in the stacking process. To further enhance the device efficiency, the use of phosphorescent emitting materials is necessary due to their high internal quantum efficiency. Recently, a much higher efficiency than that of polymer materials was reported for solution-processed phosphorescent OLEDs with small-molecule materials [90, 91]. These high efficiencies were comparable to the conventional vacuum-evaporated phosphorescent OLEDs. The application of small-molecule and phosphorescent emitting materials in solution-processed devices will become an even more important challenge.

In the final section, we will describe solution-processed tandem OLEDs comprising two phosphorescence-based LEUs with phosphorescent small-molecule emitting dopants, small-molecule host materials, and a polymer material as a binder to improve the insolubility of the LEU films [92]. A bilayer of ZnO and PEIE serves as an efficient EIL in each LEU, and poly(3,4-ethylenedioxythiophene):poly(styrenesulfonate) (PEDOT:PSS) has been used as an interconnecting transparent conductive layer (Fig. 8a). The reaction between ZnO and PSS due to the acidity of PSS does not allow ZnO to be uniformly spin coated onto a pristine PEDOT:PSS layer. Therefore, a neutralized PEDOT:PSS layer has to be inserted between the pristine PEDOT:PSS layer and ZnO nanoparticles to prevent direct contact between them. The multilayer structure PEDOT:PSS/neutralized PEODT:PSS/ZnO/PEIE structure is not soluble in common organic solvents such as toluene, *p*-xylene, and tetrahydrofuran. In a phosphorescent LEU, poly(9-vinylcarbazole) (PVK), 4,4′,4″-tris(carbazol-9-yl)-triphenylamine (TCTA), and 2,6-bis(3-(9-carbazol-9-yl)phenyl)-pyridine (26DCzppy) are used in the host materials. Phosphorescent dopants such as tris(2-(4,6-difluorophenyl)pyridine)iridium(III) ($Ir(Fppy)_3$), tris(2-phenylpyridine)iridium(III) ($Ir(ppy)_3$), and tris(2-phenyl-1-quinoline)pyridine)iridium(III) ($Ir(phq)_3$) are used as the blue, green, and red emitter of LEUs as shown in Fig. 8b. Mixed small-molecule host materials of TCTA and 26DCzppy for the green

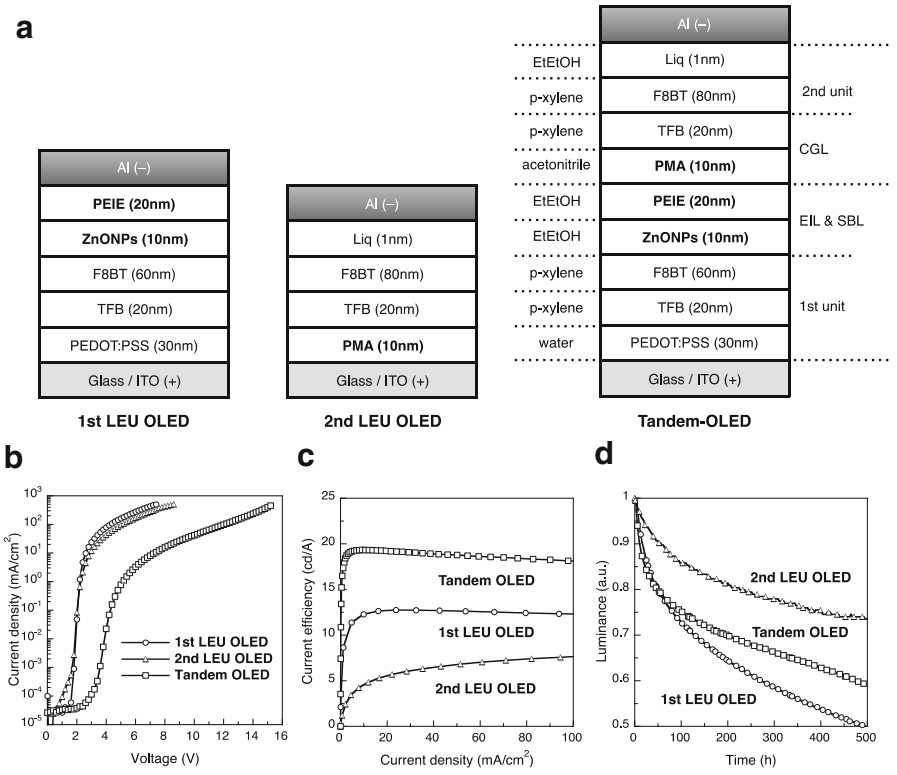

Fig. 7 **a** Device structure of the 1st LEU OLED, 2nd LEU OLED, and fully solution-processed fluorescent light-emitting polymer-based tandem OLED. **b** Current efficiency–current density characteristics of the devices. **c** Operational lifetime of the devices at the same current density (7.5 mA/cm^2). Initial luminances were 800 cd/m^2 for the 1st LEU, 300 cd/m^2 for the 2nd LEU and 1200 cd/m^2 for the tandem OLED. Reproduced with permission from [89]. Copyright 2014, WILEY-VCH Verlag GmbH & Co. KGaA, Weinheim

phosphorescent dopant are known to be as an effective approach to obtain high device efficiency. TCTA has a role in hole injection and transport. 26DCzppy is a bipolar transport host material with a high triplet energy level for phosphorescent devices, improving the balance of holes and electrons. The large difference in the surface energies makes it challenging to uniformly coat PEDOT:PSS from its aqueous dispersion onto a hydrophobic organic layer. The addition of methanol and 2-propanol into the aqueous PEDOT:PSS dispersion allows PEDOT:PSS to be coated uniformly over the EML. However, the use of an aqueous solution over the EML comprising only the small molecules TCTA, 26DCzppy, and Ir(ppy)$_3$ over the EML results in the penetration of aqueous solvent through the EML and, consequently, in the dissolution of the PEIE and ZnO layers. Thus, to prevent the dissolution of PEIE and ZnO in the aqueous solvent, PVK is added into the EML to serve as a binder host, resulting in the formation of a uniform multilayered structure of ZnO/PEIE/EML/PEDOT:PSS. A careful choice of the coating solvents and

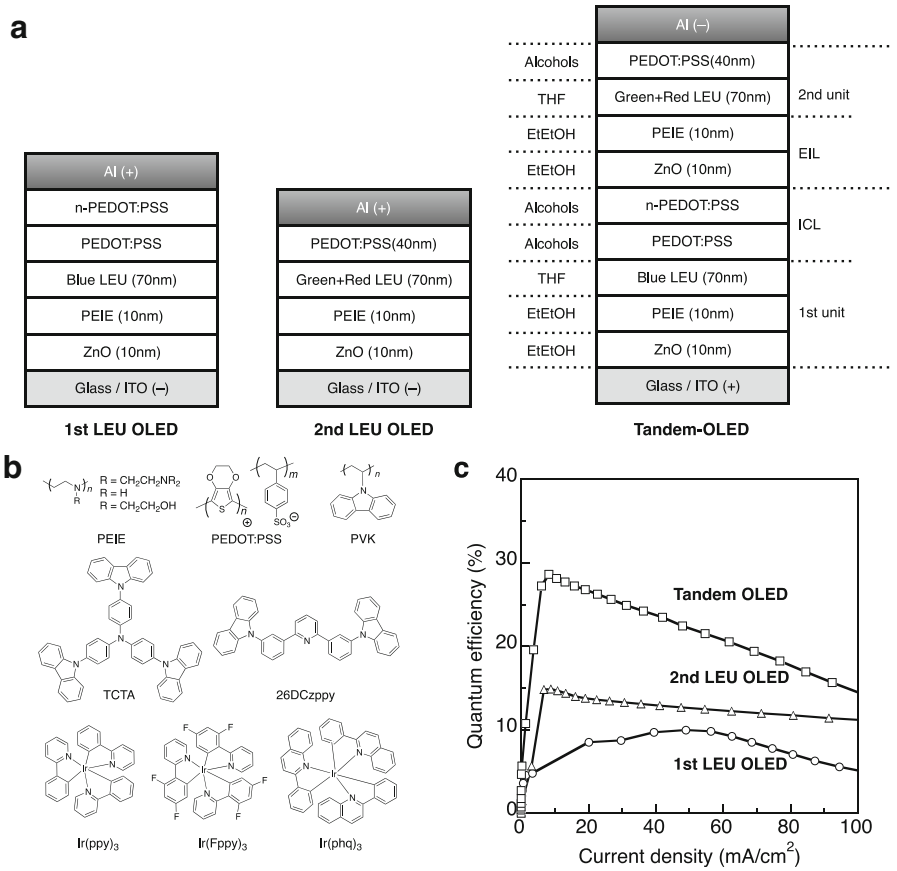

Fig. 8 **a** Device structures of 1st LEU, 2nd LEU, and inverted white phosphorescent tandem OLEDs. **b** Chemical structures of the materials. **c** External quantum efficiency–current density characteristics of the devices. Reproduced with permission from [92]. Copyright 2015, WILEY-VCH Verlag GmbH & Co. KGaA, Weinheim

materials ensured orthogonal solubilities for materials used in adjacent layers; any loss of material during rinsing is indicated by a reduction in the absorbance. A white phosphorescent tandem OLED was fabricated by stacking blue and green/red LEUs. The white emission was quite stable with the current density, and the efficiencies reached up to 69 cd/A and 28 % EQE at 5000 cd/m^2 (Fig. 8c). The successful fabrication of tandem OLEDs with an inverted structure using solution-based processes will pave the way towards printable, low-cost, and large-area white light sources.

6 Conclusion

We focused our attention on the tandem structure of OLEDs including the interconnecting layer (TCLs or CGLs) and EILs. In conventional OLEDs, the operational lifetime decreases with increasing luminance due to the degradation of the organic materials caused by charge under a high current density. However, the tandem structure of OLEDs comprising individual LEUs, EILs, and an interconnecting layer can avoid the tradeoff between a long operational lifetime and high luminance (or current density). For two-LEU stacked tandem OLEDs, the luminance and driving voltage increased two-fold compared to those of single LEU OLEDs under an identical current density condition. Therefore, the efficiencies of tandem OLEDs exhibits a two-fold increase compared with single LEU OLEDs. In addition, at the same luminance, the operational lifetime of tandem OLEDs is also longer than that of single LEU OLEDs. This is due to the reduced current density in each individual LEU.

Several types of interconnecting layers for tandem OLEDs have been reported: (1) transparent conductive electrode type using ITO or ultra-thin metals, (2) electron-accepting and electron-donating bilayers as the CGL, and (3) *n*- and *p*-type organic heterojunction CGL type. In particular, various electron-accepting materials such as Lewis acid ($FeCl_3$, F_4TCNQ), *n*-type metal oxides (MoO_3, WO_3), and *n*-type organic $HATCN_6$ have been demonstrated. These electron-accepting materials can effectively accept an electron from the HOMO level of electron-donating materials. Three types of EILs in tandem OLEDs have also been reported using alkali metals containing *n*-dopants (Cs, Cs_2CO_3, and CsN_3), a bilayer of alkali metal halides (LiF, Liq)/metals (Al), and organic-based *n*-type dopants. These EILs can reduce the electron injection barrier between LEU and CGL due to the resulting energy level alignment.

Finally, recent progress in solution-processed tandem OLEDs and solution-processed EILs and CGLs was also discussed. An appropriate choice of coating solvents for each layer ensures a multilayered structure produced using solution-based processes. Fluorescent light-emitting polymer-based tandem OLEDs comprising ZnO/PEIE as an EIL and PMA as an electron acceptor of the CGL exhibit a doubled efficiency and a longer operational lifetime when compared with single LEU OLEDs. Phosphorescent-based solution-processed tandem OLEDs can achieve a high efficiency (28 % EQE), even with a high luminance.

References

1. Kido J, Kimura M, Nagai K (1995) Science 267:1332
2. Shen ZL, Burrows PE, Bulovic V, Forrest SR, Thompson ME (1997) Science 276:2009
3. Sun Y, Giebink NC, Kanno H, Ma B, Thompson ME, Forrest SR (2006) Nature 440:908
4. Reineke S, Lindner F, Schwartz G, Seidler N, Walzer K, Lussem B, Leo K (2009) Nature 459:234
5. Helander MG, Wang ZB, Qiu J, Greiner MT, Puzzo DP, Liu ZW, Lu ZH (2011) Science 332:944
6. Han T-H, Lee Y, Choi M-R, Woo S-H, Bae S-H, Hong BH, Ahn J-H, Lee T-W (2012) Nat. Photon. 6:105

7. Uoyama H, Goushi K, Shizu K, Nomura H, Adachi C (2012) Nature 492:234
8. Meerheim R, Walzer K, Pfeiffer M, Leo K (2006) Appl Phys Lett 89:061111
9. T. Matsumoto, T. Nakada, J. Endo, K. Mori, N. Kawamura, A. Yokoi, J. Kido (2003) SID 03 Digest 979
10. Liao LS, Klubek KP, Tang CW (2004) Appl Phys Lett 84:167
11. Kanno H, Holmes RJ, Sun Y, Kena-Cohen S, Forrest SR (2006) Adv Mater 18:339
12. Liao LS, Slusarek WK, Hatwar TK, Ricks ML, Comfort DL (2008) Adv Mater 20:324
13. Chiba T, Pu Y-J, Miyazaki R, Nakayama K-I, Sasabe H, Kido J (2011) Org Electron 12:710
14. Lee S, Shin H, Kim JJ (2014) Adv Mater 26:5864
15. Zhang Y, Lee J, Forrest SR (2014) Nat Commun 5:5008
16. Law CW, Lau KM, Fung MK, Chan MY, Wong FL, Lee CS, Lee ST (2006) Appl Phys Lett 89:133511
17. Chan MY, Lai SL, Lau KM, Fung MK, Lee CS, Lee ST (2007) Adv Funct Mater 17:2509
18. Hamwi S, Meyer J, Kroger M, Winkler T, Witte M, Riedl T, Kahn A, Kowalsky W (2010) Adv Funct Mater 20:1762
19. Yang JP, Xiao Y, Deng YH, Duhm S, Ueno N, Lee ST, Li YQ, Tang JX (2012) Adv Funct Mater 22:600
20. Liu J, Huang SJ, Shi XD, Wu XK, Wang J, He GF (2013) J Phys Chem C 117:13887
21. Sun JX, Zhu XL, Peng HJ, Wong M, Kwok HS (2005) Appl Phys Lett 87:093504
22. Zhang HM, Dai YF, Ma DG, Zhang HM (2007) Appl Phys Lett 91:123504
23. Zhang HM, Choy WCH, Dai YF, Ma DG (2009) Org Electron 10:402
24. Ding BF, Hou XY, Alameh K (2012) Appl Phys Lett 101:133305
25. Liao LS, Klubek KP (2008) Appl Phys Lett 92:223311
26. Terai M, Tsutsui T (2007) Appl Phys Lett 90:083502
27. Yan F, Chen R, Sun HD, Sun XW (2013) Appl Phys Lett 102:203303
28. Tsutsui T, Terai M (2004) Appl Phys Lett 84:440
29. Guo FW, Ma DG (2005) Appl Phys Lett 87:173510
30. Chen CW, Lu YJ, Wu CC, Wu EHE, Chu CW, Yang Y (2005) Appl Phys Lett 87:241121
31. Kanno H, Giebink NC, Sun YR, Forrest SR (2006) Appl Phys Lett 89:023503
32. Ho MH, Chen TM, Yeh PC, Hwang SW, Chen CH (2007) Appl Phys Lett 91:233507
33. Lee TW, Noh T, Choi BK, Kim MS, Shin DW, Kido J (2008) Appl Phys Lett 92:043301
34. Yook KS, Jeon SO, Min SY, Lee JY, Yang HJ, Noh T, Kang SK, Lee TW (2010) Adv Funct Mater 20:1797
35. Sasabe H, Minamoto K, Pu YJ, Hirasawa M, Kido J (2012) Org Electron 13:2615
36. Zhao YB, Tan ST, Demir HV, Sun XW (2015) Org Electron 23:70
37. Chang CC, Chen JF, Hwang SW, Chen CH (2005) Appl Phys Lett 87:253501
38. Leem DS, Lee JH, Kim JJ, Kang JW (2008) Appl Phys Lett 93:103304
39. Gao CH, Zhu XZ, Zhang L, Zhou DY, Wang ZK, Liao LS (2013) Appl Phys Lett 102:153301
40. Zhou DY, Cui LS, Zhang YJ, Liao LS, Aziz H (2014) Appl Phys Lett 105:153302
41. Zhou DY, Zu FS, Zhang YJ, Shi XB, Aziz H, Liao LS (2014) Appl Phys Lett 105:083301
42. Ding L, Tang X, Xu MF, Shi XB, Wang ZK, Liao LS (2014) Acs Appl Mater Interfaces 6:18228
43. Sun HD, Guo QX, Yang DZ, Chen YH, Chen JS, Ma DG (2015) Acs Photonics 2:271
44. Zhou DY, Shi XB, Liu Y, Gao CH, Wang K, Liao LS (2014) Org Electron 15:3694
45. Kroger M, Hamwi S, Meyer J, Riedl T, Kowalsky W, Kahn A (2009) Appl Phys Lett 95:123301
46. Meyer J, Kroger M, Hamwi S, Gnam F, Riedl T, Kowalsky W, Kahn A (2010) Appl Phys Lett 96:193302
47. Kim YK, Kim JW, Park Y (2009) Appl Phys Lett 94:063305
48. Lai SL, Chan MY, Fung MK, Lee CS, Lee ST (2007) J Appl Phys 101:014509
49. Chen YH, Wang Q, Chen JS, Ma DG, Yan DH, Wang LX (2012) Org Electron 13:1121
50. Liu HH, Yan F, Wang H, Miao YQ, Du XG, Jing S, Gao ZX, Chen LQ, Hao YY, Xu BS (2013) Appl Phys Lett 102:013304
51. Lu ZY, Li X, Wang Y, Xiao J, Xu PL (2014) Curr Appl Phys 14:1465
52. Hong K, Lee JL (2012) J Phys Chem C 116:6427
53. Hung LS, Tang CW, Mason MG (1997) Appl Phys Lett 70:152
54. Cho K, Cho SW, Jeon PE, Lee H, Whang CN, Jeong K, Kang SJ, Yi Y (2008) Appl Phys Lett 92:093304
55. Ding BF, Alameh K (2012) J Phys Chem C 116:24690
56. Endo J, Matsumoto T, Kido J (2002) Jpn J Appl Phys 41:L800

57. Pu Y-J, Miyamoto M, Nakayama K, Oyama T, Masaaki Y, Kido J (2009) Org Electron 10:228
58. Friend RH, Gymer RW, Holmes AB, Burroughes JH, Marks RN, Taliani C, Bradley DDC, Dos Santos DA, Bredas JL, Logdlund M, Salaneck WR (1999) Nature 397:121
59. Ho PKH, Kim JS, Burroughes JH, Becker H, Li SFY, Brown TM, Cacialli F, Friend RH (2000) Nature 404:481
60. Burn PL, Lo SC, Samuel IDW (2007) Adv Mater 19:1675
61. Gong X, Wang S, Moses D, Bazan GC, Heeger AJ (2005) Adv Mater 17:2053
62. Huang F, Zhang Y, Liu MS, Jen AKY (2009) Adv Funct Mater 19:2457
63. Earmme T, Ahmed E, Jenekhe SA (2010) Adv Mater 22:4744
64. Yang X, Müller DC, Neher D, Meerholz K (2006) Adv Mater 18:948
65. Niu YH, Liu MS, Ka JW, Bardeker J, Zin MT, Schofield R, Chi Y, Jen AKY (2007) Adv Mater 19:300
66. Png RQ, Chia PJ, Tang JC, Liu B, Sivaramakrishnan S, Zhou M, Khong SH, Chan HS, Burroughes JH, Chua LL, Friend RH, Ho PK (2010) Nat Mater 9:152
67. Huang JS, Li G, Wu E, Xu QF, Yang Y (2006) Adv Mater 18:114
68. Huang J, Xu Z, Yang Y (2007) Adv Funct Mater 17:1966
69. Earmme T, Jenekhe SA (2012) Adv Funct Mater 22:5126
70. Qian L, Zheng Y, Choudhury KR, Bera D, So F, Xue JG, Holloway PH (2010) Nano Today 5:384
71. Youn H, Yang M (2010) Appl Phys Lett 97:243302
72. Chiba T, Pu Y-J, Hirasawa M, Masuhara A, Sasabe H, Kido J (2012) Acs Appl. Mater. Interfaces 4:6104
73. Bolink HJ, Brine H, Coronado E, Sessolo M (2010) Adv Mater 22:2198
74. Kabra D, Lu LP, Song MH, Snaith HJ, Friend RH (2010) Adv Mater 22:3194
75. Vaynzof Y, Kabra D, Chua LL, Friend RH (2011) Appl Phys Lett 98:113306
76. Park JS, Lee JM, Hwang SK, Lee SH, Lee HJ, Lee BR, Park HI, Kim JS, Yoo S, Song MH, Kim SO (2012) J Mater Chem 22:12695
77. Chiba T, Pu Y-J, Sasabe H, Kido J, Yang Y (2012) J Mater Chem 22:22769
78. Talik NA, Yeoh KH, Ng CYB, Yap BK, Woon KL (2014) J Lumin 154:345
79. Akatsuka T, Roldan-Carmona C, Orti E, Bolink HJ (2014) Adv Mater 26:770
80. Zhou Y, Fuentes-Hernandez C, Shim J, Meyer J, Giordano AJ, Li H, Winget P, Papadopoulos T, Cheun H, Kim J, Fenoll M, Dindar A, Haske W, Najafabadi E, Khan TM, Sojoudi H, Barlow S, Graham S, Bredas JL, Marder SR, Kahn A, Kippelen B (2012) Science 336:327
81. Kim YH, Han TH, Cho H, Min SY, Lee CL, Lee TW (2014) Adv Funct Mater 24:3808
82. Hofle S, Schienle A, Bruns M, Lemmer U, Colsmann A (2014) Adv Mater 26:2750
83. Stolz S, Scherer M, Mankel E, Lovrincic R, Schinke J, Kowalsky W, Jaegermann W, Lemmer U, Mechau N, Hernandez-Sosa G (2014) Acs Appl. Mater Interfaces 6:6616
84. Chen S, Manders JR, Tsang SW, So F (2012) J Mater Chem 22:24202
85. Hofle S, Bruns M, Strassle S, Feldmann C, Lemmer U, Colsmann A (2013) Adv Mater 25:4113
86. Hofle S, Schienle A, Bernhard C, Bruns M, Lemmer U, Colsmann A (2014) Adv Mater 26:5155
87. Hofle S, Bernhard C, Bruns M, Kubel C, Scherer T, Lemmer U, Colsmann A (2015) Acs Appl. Mater. Interfaces 7:8132
88. Aizawa N, Pu Y-J, Chiba T, Kawata S, Sasabe H, Kido J (2014) Adv Mater 26:7543
89. Pu Y-J, Chiba T, Ideta K, Takahashi S, Aizawa N, Hikichi T, Kido J (2015) Adv Mater 27:1327
90. Aizawa N, Pu Y-J, Watanabe M, Chiba T, Ideta K, Toyota N, Igarashi M, Suzuri Y, Sasabe H, Kido J (2014) Nat. Commun. 5:5756
91. Perumal A, Faber H, Yaacobi-Gross N, Pattanasattayavong P, Burgess C, Jha S, McLachlan MA, Stavrinou PN, Anthopoulos TD, Bradley DDC (2015) Adv Mater 27:93
92. Chiba T, Pu Y-J, Kido J (2015) Adv Mater 27:4681